Fan-Beam Based Virtual Fluoroscopy for Navigated Catheterization in Interventional Radiology

Pierrick Guiral[a], Patrick Pittet[b], Yannick Grondin[c], Patrice Jalade[d], Jean-Marc Galvan[b], Guo-Neng Lu[b], Laurent Desbat[a], Philippe Cinquin[a]

[a] *Univ. Grenoble Alpes, CNRS, Grenoble INP, TIMC-IMAG, F-38000 Grenoble, France*
[b] *Université de Lyon, CNRS, Université Lyon 1, INL, F-69100 Villeurbanne, France*
[c] *SurgiQual Institute, F-38240 Meylan, France*
[d] *HCL, Centre Hospitalier Lyon Sud, Service de Radiophysique et Radiovigilance, F-69310 Pierre-Bénite, France*

Abstract

Personalized medicine implies reducing invasiveness of therapeutic procedures. Although interventional radiology proved a very interesting alternative to surgical procedures, it still raises concerns due to the irradiation dose received by the medical team (and by the patient). We propose a novel concept allowing to reduce very significantly the irradiation dose during the phases where tools inserted in the patient have to be tracked with respect to previously acquired images. This implies inserting a miniaturized X-ray detector in the tip of the tools, and reducing the dose by a "rotating collimator". We demonstrate that real-time processing of the signals allows accurate localization of the tip of the tools, with a dose reduction of at least ten times.

Keywords:

Image Processing, Computer-Assisted; Radiology, Interventional; Catheterization

Introduction

Interventional radiology is nowadays widely used in many medical fields such as cardiology, neurology, vascular surgery, gastroenterology, urology, gynaecology and orthopedics. In 2010, 545,000 interventional radiology (IR) procedures were reported in France for both diagnoses and treatments [1]. The benefits of interventional radiology are numerous and well established.

Among these procedures, catheterization consists in introducing a catheter in the patient's body through arteries or vessels to a certain region of the body for diagnostic or therapeutic purposes. Catheterization is a delicate procedure and it is most often performed under continuous 2D X-ray imaging, i.e. fluoroscopy guidance, to help the physician localize the catheter tip in the vascular system.

However, since fluoroscopy is performed each time the catheter moves, the staff (mostly the operating physician) and the patient can be significantly exposed to ionizing radiations, particularly in long procedures. Deterministic effects threshold due to high doses may be reached in such long procedures [2].

To follow the guidelines of the ALARA principle (As Low As Reasonably Achievable) [3], there has been a proposed approach for fluoroscopy guidance to reduce the dose received by staff and patients during IR procedures [4]. As compared to conventional fluoroscopy guidance which implements an X-ray cone beam, this approach suggests Virtual Fluoroscopy (VF)

guidance based on a rapid scanning of the imaging field by an X-ray fan beam.

In this paper, we report the implementation of this approach as a proof of concept. Firstly, the operating principle of the method and its implementation are described. Then, the in-vitro exprimentation carried out in clinical conditions is presented. Finally, measured results are analyzed and discussed before conclusion.
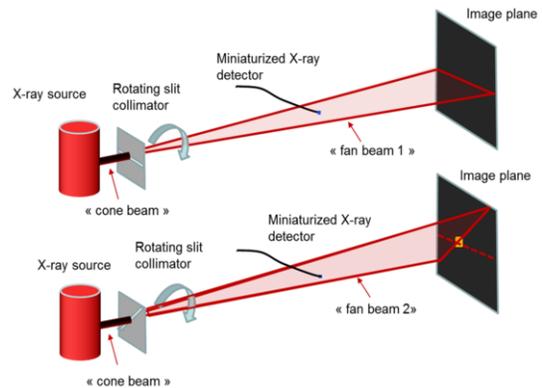

Figure 1 – Principle of the Proposed Virtual Fluoroscopy Method Based on X-Ray Fan Beam Scanning of the Imaging Field

Methods

Operating Principle

The proposed VF approach makes use of an X-Ray fan-beam to scan the image field during each fluoroscopy pulse. A rotating-slit collimator is positioned at the cone beam output of the X-ray tube. This allows the obtaining of a rotating fan beam, as illustrated in Figure 1. A miniaturized real-time X-ray detector in a guidewire is placed between the slit collimator and the image panel. The rotation speed of the collimator disk is set to be equal to the fluoroscope pulse rate. During the fan beam scan of the image field, the detector probe is irradiated two times at two specific brief moments corresponding to two projected slit positions on the image plane, $l_1(t_1)$ and $l_2(t_2)$. By detecting the detector-irradiated moments t_1 and t_2, one can determine the detector position projected in the image plane. Figure 1.a and b illustrates the two detected moments t_1 and t_2,

with corresponding slit projections l_1 and l_2 in the image plane. By calculating intersection of l_1 and l_2, the detector position projected in the collimator plane, x, is first determined and then, the corresponding position in the image plane, x', is obtained by projection along the line defined by x and the X-ray source focus. Thus, during the IR procedure, the detector position can be real-time displayed at the fluoroscopy pulse rate.

Implementation

Figure 2 implements this VF approach using several major parts presented as follows.
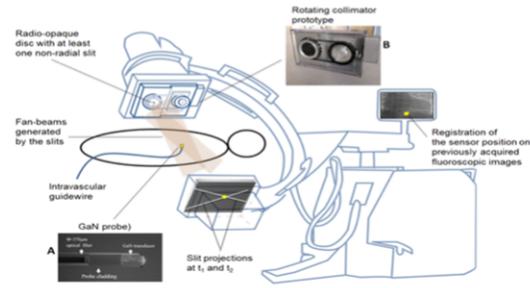

Figure 2 – Implementation of Virtual Fluoroscopy Guidance

Rotating Slit Collimator

The collimator is a 1mm-thick disk, made of Cadmium Tungstate (CdWO4), a high-density material (2'' wafer from Saint Gobain Cristal). It is noted that 1mm-thick CdWO4 absorbs more than 95% of the photon fluency at 100 keV. Moreover, CdWO4 is a scintillator with relatively high light yield, and its prompt luminescence can be detected for the synchronization of the collimator rotation on the fluoroscopy pulse rate.

The disc has a single off-axis straigth-line slit positioned at a distance R=2mm from its axis, as shown in Figure 3. The slit has a width of 220μm. The collimator is driven using a brushless motor (80280007, Crouzet, France) for a rotation speed up to 3000rpm (which corresponds to a fluoroscopy pulse duration down to 20 ms).
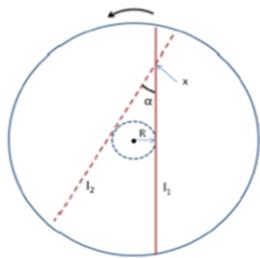

Figure 3 – Design of a Collimator with a Single Off-Axis Slit

Miniaturized Detector Probe

The detector probe is made of a small-volume Gallium Nitride (GaN) radioluminescent (RL) transducer and a coupled optical fiber to collect RL signal and to transmit it to a photodetection module. The GaN transducer has a very high RL yield with a response time in the order of ns [5]. The use of a small volume GaN transducer can produce detectable RL signal, which is suitable for designing a miniaturized detector probe.

The designed detector probe has an outer diameter smaller than 400μm, incorporating at its tip end a Si-doped GaN crystal of ~0.1mm³ (Saint Gobain Cristals, France).

The detector probe is connected to a photodetection module for its operation. The associated photodetection module mainly consists of a photon counting head (H10682-210, Hamamatsu photonics Corp., Japan). It outputs a pulse of 10ns-width per photon and provides a pulse-pair resolution of 20ns. This signal is processed in real time by an FPGA-based processing unit.

This unit is designed to perform differents tasks: i) synchronous real-time processing of detected signal (sliding counting window of 100μs with a 10 μs resolution), ii) motor speed control and iii) instantaneous collimator position tracking.

System for In-Vitro Testing

Figure 4 illustrates a VF testing system making use of different designed parts presented above. It employs a cylindrical Plexiglas Phantom of 12cm in diameter. The detector probe is placed on the axis of this phantom. The X-ray cone beam comes from the kV On-Board-Imager (OBI) embedded on the radiotherapy system (Truebeam, Varian, Inc) installed at Centre Hospitalier Lyon Sud. This clinical equipment allows accurate positioning and alignment of the collimator and the phantom. OSL dosimeters are also employed at the top surface of the phantom for absolute dose measurements.
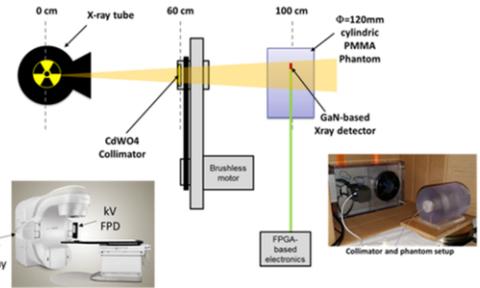

Figure 4 – System for In-Vitro Testing

Results

Dose Reduction

The proposed VF approach allows dose reduction by the ratio between the fan-beam field and the cone-beam field. By assuming an homogeneous dose in the cone beam field (i.e. $D_{CB} \sim constant$), the dose at a given Point of Interest (POI) in the fan beam field can be expressed in function of the cone-beam dose as:

$$\begin{cases} D_{FB}(r) \sim D_{CB} \dfrac{cos^{-1}\left(\frac{R-0.5w}{r}\right) - cos^{-1}\left(\frac{R+0.5w}{r}\right)}{\pi} \, for \, r > R \\ D_{FB}(r) = 0 \, for \, r \leq R \end{cases} \quad (1)$$

where w is the width of the slit.

Figure 5 shows the virtual fluoroscopy dose evaluated according to equation 1.

Due to the off-axis position of the slit in the collimator, central area of the field is never exposed (blind area). For any POI positioned at an off-axis distance larger 2.5mm, the calculated dose behind the collimator is more than 20 times smaller than the one in front of the collimator.

Experimentally, we acquired images with the OBI X-ray imaging system while the collimator was in rotation at 1000rpm. We used a high dose setting of the tube to obtain a signal strong enough on the imager (i.e. 70kV, 155mA, 644ms). An X-ray image is shown in Figure 5 as well as the grey level profile along the yellow line. The central black disk of 4mm in diameter corresponds to the blind area. The bright white ring surrounding this area is due to the quasi-tangential position of the slit for these positions. The measured grey level profile is very consistent with the calculated profile shown in Figure 6.
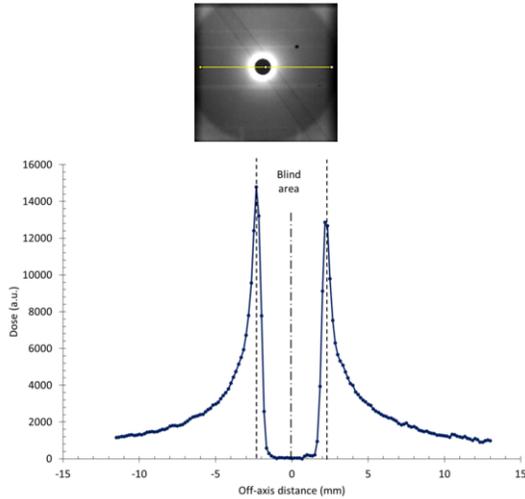

Figure 5 – Off-Axis Dose Variation Evaluated on the Rotating Collimator Image with the Gray Levels Profile Measured Along the Yellow Line

The absolute doses were measured by using the nanoDot OSL dosimeters (Landauer Inc, USA). Each consists of a 5mm diameter, 200μm thick Al2O3:C disk. The dosimeters were placed at distances D1=8mm and D2=18mm from the collimator rotation axis, on the top surface of the phantom. Each dosimeter was exposed for 10 images (70kV, 100mAs per image). The doses measured without the collimator were of 64mSv and of 62mSv for D1 and D2 positions, respectively. The dose with the collimator in operation (at 1000 rpm) decreased down to 984μSv and 681μSv, respectively. It corresponds to a dose reduction by a factor of 66 and 94 for D1 and D2, respectively.
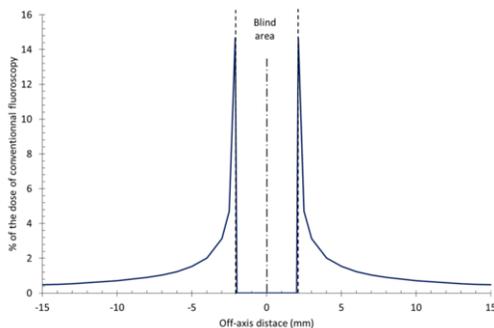

Figure 6 – Evaluated Fan-Beam Dose Versus the Off-Axis Distance of the POI (expressed as percentage of the cone beam dose)

Detection of the X-Ray Detector Probe Exposure

We placed the X-ray detector probe at a depth of 60 mm in the PMMA phantom and successively at 4mm, 7mm, and 12mm from the rotation axis (projected positions in the collimator plane). The obtained images and results are shown in Figure 7. The collimator rotation speed was set at 1000rpm and 1500rpm, respectively.
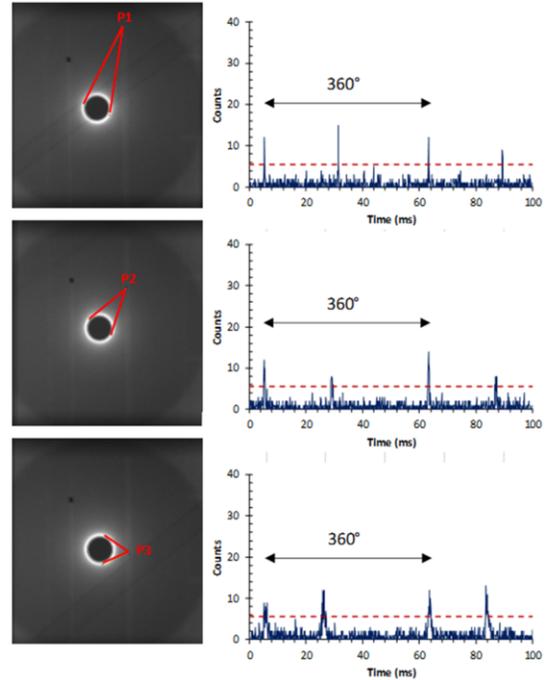

Figure 7 – X-ray Detector Probe Signal for Probes Placed at 60mm Depth in the PMMA Phantom and at Distances of a) 4mm, b) 7mm and c) 12mm from the Rotation Axis.

Figure 7 shows the signal acquired for the 3 detector probe positions. The noise floor is much higher than the dark count noise of the detector but remains sufficiently low to identify the signal peaks resulting from the detector irradiation. The slit rotation speed can be measured as the time between the ith and $(i+2)^{th}$ peaks. It was measured at ~58ms/turn (i.e. 1035rpm) and ~38ms/turn (i.e. 1569rpm) for 1000rpm and 1500rpm setups, respectively.

The time between two successive peaks linearly depends on the collimator rotation angle, β required to move from slit position l_1 to the l_2 position. The angle between these two slits positions is given by $\alpha = \pi - \beta$. The radial distance of the detector from the rotation axis is given by $r = \frac{R}{\sin(\alpha)}$. We also extracted the value of α from the images shown in Figure 7. Results are shown in Table 1. For the different tests (3 probe positions and 2 collimator rotation speeds), the α values obtained by signal and image processing are consistent.

Discussion

Collimator Optimization

The testing results confirm significant dose reduction (from one to two orders of magnitudes). However, with the proposed slit

Table 1 – Results Summary

	Time /rotation (ms)	Rotation speed (rpm)	Time between consecutive probe exposures (ms)		Signal processing			Image analysis	
			Mean	Standard deviation	Rotation Angle	Alpha	Estimated radial position (mm)	Alpha	Estimated radial position (mm)
Position P1	57.9	1035	261.1	0.8	162.2°	17.8°	12.9	18.7°	12.3
	38.4	1561	171.4	4.1	160.5°	19.5°	11.8		
Position P2	57.9	1036	237.4	2.3	147.5°	32.5°	7.2	32.0°	7.3
	38.2	1571	156.8	4.8	147.8°	32.2°	7.2		
Position P3	58.1	1034	203.0	2.5	125.9°	54.1°	4.4	58.6°	4.1
	38.1	1575	132.8	7.9	125.5°	54.5°	4.4		

geometry, the dose reduction factor strongly depends on the distance of the POI from the collimator rotation axis. Thus, the dose profile versus the distance from the rotation axis (see Figures 5 and 6), show two asymptotic trends, a steep dose gradient for distances close to the slit off-axis distance and low slope for larger distances. One possible improvement may be to propose two slits as shown in Figure 8, to prevent significant dose exposure at POI close to the off_axis position of the slits. For instance, for an off-axis distance of $R = 2mm$, it could be suitable to use slits without any aperture closer than 3mm from the rotation axis. This geometry will increase the blind area (6mm in diameter instead of 4mm with the single slit geometry) but will guarantee a more homogeneous dose over the imaging field.
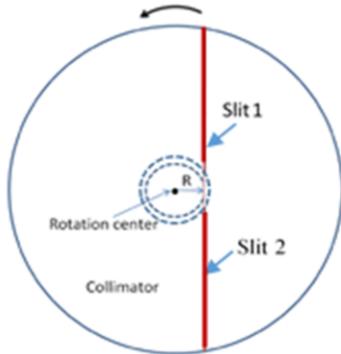

Figure 8 – Optimized Collimator Geometry with Two Off-Axis Slits

Miniaturized X-ray Detector Sensitivity

The GaN-based detector probe was operated in photon counting mode over a 100μs window. With the OSL dosimeter, we measured at the surface of the phantom a dose of 681μSv for an X-ray irradiation lasting 6440ms (10 images), i.e. a dose of ~10nSv over the counting window of 100μs. Moreover, the GaN transducer was placed at 60mm depth in the phantom where the X-ray fluence was only 19% of the fluence at the phantom surface (for the considered 70kV X-ray beam). Thus, a dose of less than 2nSv at the level of the GaN-transducer was sufficient to give more than 6 counts at the output of the detector as shown in Figure 7. This shows that the GaN-based miniaturized X-ray detector has a suitable sensitivity and a bandwidth well adapted to the VF application. Some optimizations remain to be done for contrast enhancement since the signal baseline was much higher than the dark count rate of

the detector: this could be due to an insufficient shielding against radiations or parasitic scintillation light. It is worth mentioning that the corresponding dose behind the phantom, i.e. at 120mm depth was ~0.4nSv for 100μs and was not suffficient to activate the flat panel detector at this time resolution.

Conclusions

The VF method for IR procedures has been implemented and tested. The experimental results have shown that the dose can be reduced by one or two order of magnitudes by the use of a rotating slit collimator. Further studies need to be carried out on fluoroscopy clinical systems to assess dose reduction and localization resolution achieved by VF guidance as compared to conventional fluoroscopy guidance. Moreover, this study

also confirms that the GaN-based miniaturized detector probe allows sufficient IN/OUT field contrast and bandwidth for this application (activated within 100μs by a dose smaller than 2nSv). These results establishes the proof of concept for the proposed VF approach. This novel method will be used for interventions such as embolization interventions, coronary angioplasty procedures, cryotherapy or radiofrequency ablations, biventricular cardioverter-defibrillator implantations. These instances represent several millions of interventions per year world-wide, so that we expect a major impact on Public Health.

Acknowledgements

References

[1] C. Etard, E. Bigand, C. Salvat, V. Vidal, J.P. Beregi, A. Hornbeck, and J. Greffier, Patient dose in interventional radiology: a multicentre study of the most frequent procedures in France, *Eur. Radiol.* **27** (2017) 4281–4290.

[2] W. Jaschke, M. Schmuth, A. Trianni, and G. Bartal, Radiation-Induced Skin Injuries to Patients: What the

Interventional Radiologist Needs to Know., *Cardiovasc. Intervent. Radiol.* **40** (2017) 1131–1140.

[3] K.J. Strauss, and S.C. Kaste, The ALARA (as low as reasonably achievable) concept in pediatric interventional and fluoroscopic imaging: striving to keep radiation doses as low as possible during fluoroscopy of pediatric patients--a white paper executive summary., *Pediatr. Radiol.* **36 Suppl 2**

[4] Y. Grondin, P. Augerat, P. Cinquin, L. Desbat, and M. Decrouez, Rotary collimator for determining the position of an element provided with sensors in an x-ray imaging system, EP3368919A1, 2016.

[5] T. Yanagida, Y. Fujimoto, and M. Koshimizu, Evaluation of Scintillation Properties of GaN, *E-Journal Surf. Sci. Nanotechnol.* **12** (2014) 396–399.

Address for correspondence

Philippe Cinquin
Philippe.Cinquin@univ-grenoble-alpes.fr